EBioMedicine 2 (2015) 1048–1062

Contents lists available at ScienceDirect

EBioMedicine

journal homepage: www.ebiomedicine.com

Research Paper

Involvement of Potassium and Cation Channels in Hippocampal Abnormalities of Embryonic Ts65Dn and Tc1 Trisomic Mice

Shani Stern [a], Menahem Segal [b], Elisha Moses [a,*]

[a] Department of Physics of Complex Systems, Weizmann Institute of Science, P.O. Box 26, Rehovot 76100 Israel
[b] Department of Neurobiology, Weizmann Institute of Science, P.O. Box 26, Rehovot 76100 Israel

ARTICLE INFO

Article history:
Received 24 March 2015
Received in revised form 24 July 2015
Accepted 28 July 2015
Available online 31 July 2015

Keywords:
Down syndrome
Ts65Dn
Tc1
Potassium currents
Potassium channels
Inward rectifiers
Reduced excitability
Hippocampus

ABSTRACT

Down syndrome (DS) mouse models exhibit cognitive deficits, and are used for studying the neuronal basis of DS pathology. To understand the differences in the physiology of DS model neurons, we used dissociated neuronal cultures from the hippocampi of Ts65Dn and Tc1 DS mice. Imaging of $[Ca^{2+}]i$ and whole cell patch clamp recordings were used to analyze network activity and single neuron properties, respectively. We found a decrease of ~30% in both fast (A-type) and slow (delayed rectifier) outward potassium currents. Depolarization of Ts65Dn and Tc1 cells produced fewer spikes than diploid cells. Their network bursts were smaller and slower than diploids, displaying a 40% reduction in $\Delta f / f_0$ of the calcium signals, and a 30% reduction in propagation velocity. Additionally, Ts65Dn and Tc1 neurons exhibited changes in the action potential shape compared to diploid neurons, with an increase in the amplitude of the action potential, a lower threshold for spiking, and a sharp decrease of about 65% in the after-hyperpolarization amplitude.

Numerical simulations reproduced the DS measured phenotype by variations in the conductance of the delayed rectifier and A-type, but necessitated also changes in inward rectifying and M-type potassium channels and in the hyperpolarization-activated cyclic nucleotide-gated (HCN) channels. We therefore conducted whole cell patch clamp measurements of M-type potassium currents, which showed a ~90% decrease in Ts65Dn neurons, while HCN measurements displayed an increase of ~65% in Ts65Dn cells. Quantitative real-time PCR analysis indicates overexpression of 40% of KCNJ15, an inward rectifying potassium channel, contributing to the increased inhibition. We thus find that changes in several types of potassium channels dominate the observed DS model phenotype.

© 2015 The Authors. Published by Elsevier B.V. This is an open access article under the CC BY-NC-ND license (http://creativecommons.org/licenses/by-nc-nd/4.0/).

1. Introduction

Down syndrome (DS) is the most abundant chromosomal abnormality in humans, affecting between 1:800 and 1:1200 of the population. People with DS have an extra copy (all or part) of chromosome 21 (trisomy 21). This presents severe health problems (Roizen and Patterson, 2003), with a moderate to severe intellectual disability. Several neurological differences characterize the DS brain, for example a smaller cerebellum and hippocampus (Pinter et al., 2001; Aylward et al., 1997) and a higher incidence of hyperactivity and epilepsy (Goldberg-Stern et al., 2001; Arya et al., 2011). The full neurological aspects of DS are not yet fully understood but are apparent at the behavioral, morphological and single neuron levels.

We used the Ts65Dn and Tc1 mouse models (Herault et al., 2012). The orthologous genes of human chromosome 21 reside in the mouse on segments of chromosomes 10, 16 and 17 (Hattori et al., 2000). The Ts65Dn mouse model (Davisson et al., 1993) contains a small reciprocal translocation chromosome with genes from chromosomes 16 and 17 (Reinholdt et al., 2011; Akeson et al., 2001), a total of about 50% of the DS genes. The Tc1 mouse model (O'Doherty et al., 2005) contains a freely segregating human chromosome 21 with about 83% of the known genes on Hsa21. This more recent "transchromosomal" mouse model is 50% mosaic, and it has been less thoroughly investigated.

At the behavioral level, developmental delays and hyperactivity were shown in Ts65Dn mice (Davisson et al., 1993), as well as several forms of learning deficits (Rueda et al., 2012; Wenger et al., 2004; Hyde et al., 2001; Demas et al., 1996; Martinez-Cue et al., 2002), for example impaired performance in the Morris water maze (Reeves et al., 1995). The Tc1 mice show decreased performance in cognitive and locomotive tasks (O'Doherty et al., 2005) along with impaired short term

Abbreviations: 1D, one-dimensional; 2D, two-dimensional; DC, direct current; DS, Down syndrome; EPSC, excitatory post synaptic current; GABA, *gamma*-aminobutyric acid; GIRK, G protein-coupled inwardly-rectifying potassium channels; HCN, hyperpolarization-activated cyclic nucleotide-gated; ROI, region of interest; RT-PCR, real time polymerase chain reaction; SEM, standard error of mean; TTX, tetrodotoxin; WT, wild type.

* Corresponding author.
E-mail address: elisha.moses@weizmann.ac.il (E. Moses).

http://dx.doi.org/10.1016/j.ebiom.2015.07.038
2352-3964/© 2015 The Authors. Published by Elsevier B.V. This is an open access article under the CC BY-NC-ND license (http://creativecommons.org/licenses/by-nc-nd/4.0/).

memory (Morice et al., 2008) and reduced exploratory behavior (Salehi et al., 2007).

At the cellular level, Ts65Dn exhibits a change in the balance of excitatory to inhibitory neurons in the neocortex, abnormal synapse morphology in the neocortex, hippocampus and dentate gyrus (Reeves, 2006; Best et al., 2012; Garner and Wetmore, 2012; Cramer and Galdzicki, 2012), developmental disruption of inhibitory synaptic transmission (Mitra et al., 2012) and hippocampal hypocellularity (Lorenzi and Reeves, 2006). GABA has been recently reported to be excitatory rather than inhibitory in the hippocampus of Ts65Dn (Deidda et al., 2015). A significant reduction in granule cell density in the DS cerebellum was reported by Baxter et al. (2000). In the Tc1 model a reduction in cerebellar volume was reported (O'Doherty et al., 2005), and altered protein profiles in the hippocampus (Ahmed et al., 2013).

Previous work identified a clear effect of enhanced $GABA_B$ inhibition at the single-cell level in the Ts65Dn mice. Elevated expression of GIRK2 channels using RT-PCR was reported (Harashima et al., 2006) in adult hippocampus, frontal cortex and substantia nigra of Ts65Dn mouse. This was linked to $GABA_B$–GIRK2 attenuation of synaptic plasticity as well as to reduced long term potentiation (LTP) and increased long term depression (LTD). A 2-fold increase in $GABA_B$ mediated currents in primary cultured hippocampal neurons was reported in Best et al. (2007). In the Tc1 model deficits in synaptic plasticity and learning along with reduced LTP in the dentate gyrus of the hippocampus were observed (O'Doherty et al., 2005).

In the present study we aimed at integrating single cell properties and network activity in dissociated cultures of Ts65Dn and Tc1 mouse models and in their respective diploid cultures. We report here that network activity was reduced and that trisomic neurons were less excitable due to an increase in inward rectifying potassium channel expression level (KCNJ6 and KCNJ15) and an increase in HCN currents. In parallel, single neurons exhibit reduced outward K currents compared to diploid neurons, related to changes in A-type, M-type and delayed rectifier channels. A NEURON (Hines and Carnevale, 1997) simulation of a DS cell with changes to these five types of ion channels successfully reproduced our experimental results. The results were usually similar for both models, so that we could characterize the DS cell through changes in several types of potassium currents.

2. Methods

2.1. Ethics Statement

Animal handling was done in accordance with the guidelines of the Institutional Animal Care and Use Committee (IACUC) of the Weizmann Institute of Science, and the appropriate Israeli law. The Weizmann Institute is accredited by AAALAC. The Weizmann Institutional Animal Care and Use Committee approved this study, conducted with hippocampal neurons.

2.2. Origin of Animals and Colony Maintenance

Original Ts65Dn females were stock B6EiC3Sn *a*/*A*-Ts(17^{16})65Dn/J Jackson catalog number 001924 (http://jaxmice.jax.org/strain/001924.html), mated with males from stock B6EiC3SnF1/J, Jackson catalog number 001875 (http://jaxmice.jax.org/strain/001875.html). The Ts65Dn strains are maintained by crossing Ts65Dn trisomic females to B6EiC3SnF1/J males. According to the Jackson data, B6EiC3SnF1/J males are a cross between C57BL/6JEiJ females and C3H/HeSnJ males. Ts65Dn litters comprise of Ts65Dn negative and Ts65Dn positive pups, and these are determined by genotyping.

Original Tc1 females were received from the lab of Elizabeth Fisher at University College London, strain Tc1/(129S8xC57Bl/6)F1. These were mated with males of strain (129S8xC57Bl/6)F1, obtained from the cross of C57Bl/6 males with females from stock 129S8/SvEvNimrJ, Jackson catalog 012809 (http://jaxmice.jax.org/strain/012809.html). The 129S8/SvEv strain is maintained by mating siblings.

2.3. Dissection

Primary cultures were prepared from hippocampi of E17 embryos following (Feinerman et al., 2005; Papa et al., 1995). Briefly, the hippocampus was dissected in chilled Leibovitz L15 medium enriched with 0.6% glucose and in the presence of 15 μg/ml gentamicin. The medium was oxygenated and the dissection carried out at 4 °C. The tissue was mechanically and enzymatically dissociated (papain) in small volumes of L15 using a fire-polished Pasteur pipette. Tissue was suspended in plating medium, consisting of 5% fetal calf serum and 5% heat-inactivated horse serum prepared in Eagle's minimal essential medium enriched with 0.6% glucose, 2 mM glutamine, and 15 μg/ml gentamicin. Neurons were plated on poly-L-lysine-coated (15 μg/ml) 13 mm round glass coverslips, (# 1, Menzel-Glazer), in 24-well culture plates at a density of 650,000 cells per well (one-dimensional), or 750,000 cells per well (two-dimensional). Four days after plating, the medium was changed to one containing 10% heat-inactivated horse serum. In addition, the first change of medium also contained a mixture of 50 μg/ml uridine, and 20 μg/ml 5′-fluoro-2 deoxyuridine, to block the proliferation of glial cells. After additional four days, medium was changed again to one containing 10% heat-inactivated horse serum alone. Thereafter one third of the medium was replaced daily. Midbrain and cortex tissue from each pup were harvested and stored at −70 °C for further genotyping. Each hippocampus is plated onto several separate coverslips immediately after dissection, so that neurons from different pups never mix. They grow in a standard incubator at 37 °C, 5% CO_2 until use (1–3 weeks in culture). Since the seeding of the cells is time sensitive, genotyping is delayed and performed separately, within the next day or two. One-dimensional cultures were grown on a "C" shape, patterned as described by Feinerman et al. (2005). The pattern was designed to allow a long propagation length concurrent with three observation points that fit in the microscope view and cover the two edges of the line and its center, see Fig. 1d and e.

Throughout this entire study, experiments were always done in pairs: For each diploid cell or culture that was measured, a similar trisomic cell or culture from the same littermate was measured. This was done to ensure that comparison is made between trisomic and diploid cultures obtained and grown with the exact same conditions.

2.4. Genotyping

DNA was extracted using the Extract-N-Amp Tissue PCR kit from Sigma (http://www.sigmaaldrich.com/life-science/molecular-biology/dna-and-rna-purification/extract-n-amp-tissue.html), for each ~5 mg piece of brain or ~0.5 cm mouse tail.

Genotyping of Ts65Dn was obtained using PCR, following one of two PCR protocols. The first PCR protocol (Lorenzi et al., 2010) is quoted by the authors to be 95–97% accurate, and was used for all imaging of $[Ca^{2+}]i$ experiments except for the ones involving baclofen and Fura-2. To verify the validity of this genotyping, we turned to a precise PCR protocol, which was available later (Reinholdt et al., 2011). We compared both protocols for 20 samples and found an agreement of 90%, with all the misses being false positives. We estimate the error to be at least 5% on our measurement, so it is consistent with the earlier estimate. The (Reinholdt et al., 2011) protocol was used for the electrophysiological measurements.

For Tc1 mice we followed the protocol supplied courtesy of the Fisher lab available in the Jackson homepage for genotyping of Tc1 (Jackson, 2010).

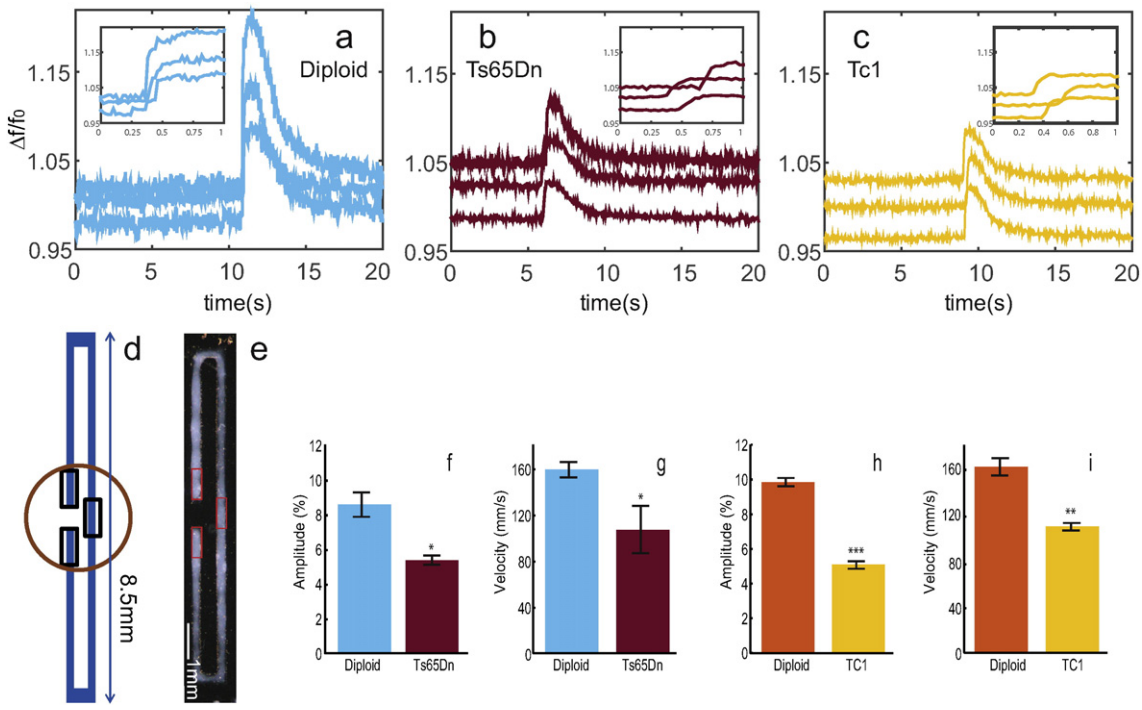

Fig. 1. Analysis of amplitude and propagation of spontaneous network bursts in one-dimensional cultures observed by imaging of $[Ca^{2+}]i$. Bicuculline was administered at 40 μM. a, Example of time course for the fluorescence signal for a diploid network, depicting the intensity measured in each of the three ROIs drawn in d. Fluorescence signals were normalized by the baseline fluorescence f_0. To improve visualization, traces are shifted relative to one another by $\pm 0.03 \frac{\Delta f}{f_0}$. Inset: Zoom in on the initiation of the network bursts, from which arrival times of the activity at each ROI was obtained. b, Similar example of fluorescence intensity signal for Ts65Dn network. Inset as in a. c, Similar example of fluorescence intensity signal for Tc1 network. Inset as in a. d, Schematic sketch of the pattern used for growing the one dimensional culture. e, Imaging of $[Ca^{2+}]i$ of background fluorescence in a linear neuronal culture. Scale bar is 1 mm. Timing of the activity in the ROIs (marked black in d and red in e) is used to measure the velocity. f, Average fluorescence intensity $(\frac{\Delta f}{f_0})$ of cultures diploid (N = 12 cultures) vs. Ts65Dn cultures (N = 5 cultures), p = 0.021. g, Average propagation velocity of diploid (N = 12 cultures) cultures vs. Ts65Dn (N = 5 cultures) cultures, p < 0.001. h, Average fluorescence intensity $(\frac{\Delta f}{f_0})$ of diploid cultures (N = 10 cultures) vs. Tc1 cultures (N = 13 cultures), p = 0.05. i, Average propagation velocity of activity in diploid cultures (N = 10 cultures) vs. Tc1 cultures (N = 13 cultures), p = 0.01. For panels f–i data are presented as mean ± SEM, * indicates p-value < 0.05, ** is p < 0.01, and *** indicates p < 0.001.

2.5. Imaging of $[Ca^{2+}]i$

Imaging of $[Ca^{2+}]i$ was implemented using 4 μg/ml cell-permeant Fluo4-AM (Invitrogen, Carlsbad, CA) dye on cultures between 9 and 24 days in vitro (DIV), as described in Feinerman et al. (2005), and imaged on an Axiovert 135TV inverted microscope (Zeiss, Oberkochen, Germany) equipped with an Andor iXon ultra EMCCD camera. The network bursts in our cultures have a typical rise time of a few tens of milliseconds and last on the order of a few seconds. Since we were interested in measuring the duration of the bursts, the camera for imaging of calcium transients was used with a relatively low sampling time of 20–100 ms, which provided a sufficient time resolution. The measured signal during activity was subtracted from the background fluorescent of the neurons, and normalized to the percent values of that background amplitude. For the Fura-2 ratiometric experiments, 2.5 μg/ml of Fura-2 pentapotassium (Sigma) was used.

2.6. One-dimensional Cultures (Imaging of $[Ca^{2+}]i$)

In the one-dimensional geometry $GABA_A$ antagonist 1(S),9(R)-(−)-bicuculline methiodide (14343 by Sigma) was used at 40 μM. Cultures generated normally 1–10 bursts in 10 min. To account for large differences in the amount of data recorded from each culture, the mean was taken as a weighted average. The weights were taken as the total number of network bursts in a 2 hour recording period per a specific culture, divided by the total amount of network bursts in all the cultures. The weighted standard deviation was then calculated. To measure the burst velocity the fluorescence activity was recorded in three ROIs located as shown in Fig. 1a. The first time point at which activity developed in each of the ROIs was detected manually. Since the signal originated in a localized area, it is always possible to identify the side where the activity began, and to measure the velocity as the signal propagates to the other side. The speed is then the length of half the culture divided by the difference in arrival times between the central ROI and the distal one.

Once the point of initiation of a burst was entered manually, the amplitude was computed by finding the maximum of the signal automatically. The baseline was computed continuously as an IIR filter of order 1 with a forgetting factor of 0.02, and the amplitude was calculated as the baseline subtracted from the maximum and then divided by the baseline $(\Delta f / f_0)$.

2.7. Two-dimensional Cultures (Imaging of $[Ca^{2+}]i$)

The burst duration was measured by manually finding the beginning and the end of the burst, i.e. when the signal departs and returns to the DC level. The burst maximum was then found automatically. The amplitude was calculated as the $(\Delta f / f_0)$.

Upon application of bicuculline the burst structure changed so that the burst decay process was complex. To avoid having to estimate the precise time at which the decay process ended, the burst duration was calculated as the full width half maximum (FWHM) of the signal. The burst amplitude calculation was unchanged.

R+(−) baclofen hydrochloride (Sigma) was used as a $GABA_B$ agonist at increasing concentrations from 0.5 μM up to 3 μM. Baclofen concentration was varied by adding incremental amounts of baclofen until cessation of network activity. The culture was equilibrated for 10 min following each administration. The network was considered to be

inactive if there were no spontaneous network bursts for 5 min following an initial 5 min recording.

The ratio of the Fura-2 baseline signal at 340 nm to the one at 380 nm, which is a measure of the internal Calcium concentration in the cell, was measured and compared between trisomic and diploid animals.

2.8. Whole Cell Patch-clamp

Neurons on glass coverslips were transferred to a recording chamber in standard recording medium, containing (in mM) 10 HEPES, 4 KCl, 2 $CaCl_2$, 1 $MgCl_2$, 139 NaCl, 10 D-glucose (340 mOsm, pH 7.4). Cells were patch-clamped with pipettes containing (in mM) 136 K-gluconate, 10 KCl, 5 NaCl, 10 HEPES, 0.1 EGTA, 0.3 Na-GTP, 1 Mg-ATP, and 5 phosphocreatine, pH 7.2 (pipette tip resistance was 5–8 MΩ). Action potentials were evoked by injecting depolarizing current pulses in current clamp mode. Spontaneous synaptic currents were recorded in voltage clamp at −60 mV with a 50 μs sampling rate. Signals were amplified with a Multiclamp700B amplifier and recorded with Clampex 9.2 software (Axon Instruments). Data was subjected to a 500 Hz low-pass filter and analyzed using Clampfit-9 and the software package Matlab (2013a, The MathWorks Inc., Natick, MA, 2000). All measurements were conducted at room temperature. A major problem with Tc1 is that they are mosaic, so that both trisomic and normal cells are combined in the measurement with no ability to separate their contributions. This necessitated more averaging for the observation of phenotypic differences in Tc1.

2.9. Network Activity, Bursts Duration and Miniature EPSCs (Electrophysiology)

Network activity was measured by holding the neurons at −60 mV and recording their currents. The burst duration was found by manually identifying the beginning and end of bursts. The amount of bursting time was calculated as the percentage of the time that the network spent in bursts during a 2 minute recording. Miniature EPSCs were recorded while blocking sodium currents by 0.5 μM TTX.

2.10. Action Potential Analysis (Electrophysiology)

Neurons were typically held near −55 mV with steady holding current, and current injections were given starting 40 pA below the steady holding current and then incremented in 20 pA current steps until action potentials were elicited. The current was then incremented in 20 pA current steps. Neurons that needed more than 100 pA to be held at −60 mV were not used in the analysis of action potentials. The analysis was performed on the first action potential produced at the lowest current step at which action potentials were evoked.

Action potential parameters: The rise time was measured as the time from the initiation of the action potential until the amplitude reached half of its maximal height. The after-hyperpolarization (AHP) amplitude was calculated as the difference between the threshold for spiking and the value of the potential 5 ms after the potential returned to cross the threshold value. The resting membrane potential was calculated as the potential at zero current. Neurons with a resting membrane potential more depolarized than −50 mV were discarded from the analysis.

The input conductance was calculated around the resting membrane potential, by measuring the current with the cell held first at −70 mV and then at −50 mV. The input conductance was calculated as: $g_{in} = \frac{\Delta I}{\Delta V} = \frac{I_{-70} - I_{-50}}{V_{-70} - V_{-50}}$, with I_{-70} and I_{-50} the respective currents measured. $V_{-70} - V_{-50}$ is the actual measured voltage difference when aiming for −70 mV and −50 mV respectively, typically close within 1 or 2 mV to −20 mV.

2.11. Single Cell Excitability

Neurons that had a resting membrane potential more depolarized than −50 mV were discarded from the analysis. To calculate the number of action potentials per depolarization step, the first depolarization step was taken as the current needed for holding the neuron closest to −55 mV. To compensate for leakage currents and to unify the statistics we assumed that the resting membrane potential is −55 mV for all cells, and therefore the current needed for this membrane potential is calibrated as zero current. Injection of currents larger than 100 pA will often cause a non-linear dynamic response as the cell cannot take such large currents. We thus did not consider values larger than 100 pA.

Linear regression was used to estimate the relation between the number of action potentials and the depolarization step. After computing two regression lines (one for trisomic cells and one for diploid cells), we compared the two lines with the aoctool linear regression program of Matlab and with the similar Comp2Regs_Pgm.php program available online. Although the relationship was not perfectly linear, this does give a good estimate on the statistical significance of the difference between the two curves.

2.12. Potassium Current Measurements

Fast and slow potassium currents were measured in the presence of 0.5 μM TTX (Alomone Labs, Jerusalem) to block sodium currents. Cells were held at −60 mV, and voltage steps of 300 ms were made in the range of −90 mV to 80 mV.

Fast potassium currents were defined as the maximum outward currents that appear a few milliseconds after the depolarization step. Slow potassium currents were measured as the outward currents at the end of the depolarization step, 300 ms after the beginning of the voltage step. The extrapolated current estimated by the channels which are open at ~0 pA (currents due to input conductance) was subtracted from the slow and fast potassium currents measured.

To account for differences arising from cell size, these currents were normalized by the estimated capacitance of the cell, estimated by: $C = \tau * g_{in}$ with τ the time it took the current to reach 1/e of its amplitude (absolute value) at the termination of the depolarization step. Low capacitance $C < 0.004$ nF was usually indicative of badly patched cells, which were discarded from the analysis. Statistical analysis was performed using aoctool linear regression program in matlab, which performs an ANOVA test.

2.13. M-type Current Measurements

Following a protocol similar to the one developed by Lamas et al. (1997), M-type currents were measured in the presence of 0.5 μM TTX to block sodium currents, and 50 μM CsCl to suppress HCN currents. Cells were held at a steady holding voltage of −20 mV (for 1 min), and 1 second test pulses delivered to −50 mV and −80 mV. This procedure was repeated after application of linopirdine. M-current was measured as the linopirdine-sensitive current in response to the step from −20 to −50 mV. The step to −80 mV, where M-current is expected to be completely deactivated, served as a control, and data were only used if the steady-state current at −80 mV did not change between control and linopirdine application by more than 15%. Since M-type currents are very small, the leakage resistance from the pipette to the extracellular medium was calculated by the current at −60 mV, $R_{leak} = \frac{-60\,mV}{I_{-60}}$. The leakage current at each voltage step was then calculated as $\frac{V_{holding}}{R_{leak}}$ and subtracted from the measured current to compensate for the leak.

2.14. HCN Sag

Following a protocol similar to Angelo and Margrie (2011), the HCN voltage sag, which is proportional to the amount of HCN current, was measured. Using current clamp mode, the cells were injected with currents to hyperpolarize the membrane potential to approximately −100 mV for 1 s. This hyperpolarization activates the HCN channels and allows an inward current, depolarizing it in the direction of the resting membrane potential and thus creating a sag in the voltage. The sag was calculated as the difference between the minimal value of the membrane potential, usually achieved around 150 ms after the beginning of the hyperpolarization step, and its value at the end of the period (after 1 s).

To verify that the sag is related to HCN currents, CsCl at 1 mM was applied after the measurement was concluded, and the voltage sag vanished completely as a result. This was performed in one diploid cell and in one Ts65Dn cell.

2.15. Quantitative Real-time PCR

Hippocampi from a total of 19 Ts65Dn pups (10 E17 and 9 P0) and 20 diploid littermates, (11 E17 and 9 P0) were used for mRNA expression level analysis by quantitative RT-PCR.

Quantitative RT-PCR was performed using the Applied Biosystems StepOne Plus system. RNA was purified using the RNeasy Plus Micro Kit by Qiagen (cat. no. 74034). cDNA was made using the High Capacity cDNA Reverse Transcription kit by Life Technologies (cat. no. 4368814). Each RT-PCR reaction contained 5 μl Taqman gene expression master mix by Life Technologies (cat. no. 4369015), 0.5 μl Taqman gene assays (KCNJ15 mouse) by Life Technologies (Mm02020346_s1), 2.5 μl RNAse free water and 2 μl cDNA containing 100 ng cDNA. All samples were run in triplicates and the GAPDH gene (Mm99999915_g1, Life Technologies) was used as an endogenous control.

2.16. Numerical Simulation

The NEURON (Hines and Carnevale, 1997) simulation environment was used to simulate a CA1 pyramidal cell based on a simulation that can be found in by Migliore (2012). The original WT neuron was built using a 3D reconstruction of 27 rat CA1 neurons (Migliore and Migliore, 2012). Inward rectifier channels were added according to a simulation by Gruber et al. (2003). The difference between a WT and a DS cell was simulated by changing the conductance of the potassium channels. The changes in delayed rectifiers (−53%) and in the A-type (−45%) channels were approximated according to our measurement of the changes in the fast and slow potassium currents. The base change in inward rectifiers (about +50%) was taken from the literature, and then adjusted to (+75%) for a better fit to the data. HCN channels (+100%) and M-type channels (−43%) were adjusted to best fit the experimental shape of the action potential and the reduction in excitability and in the potassium currents. A complete list of the simulation parameters is given in Table 2.

The number of action potentials per stimulation current step was measured under current clamp conditions ('IClamp' function of NEURON), and a graph of the neuronal excitability was created. Similarly, under voltage clamp conditions (the 'SEClamp' function) slow and fast potassium currents were measured for consecutive voltages steps.

3. Results

3.1. One-dimensional Ts65Dn and Tc1 Cultures Express Reduced Amplitude and Velocity of Network Bursts (Imaging of $[Ca^{2+}]i$)

Activity of the neurons in 1D cultures occurs in network bursts that originate in specific locations and propagate from there continuously along the line (Feinerman et al., 2005). $GABA_A$ was blocked by bicuculline, which enhanced the fluorescent signal. Fig. 1a, b and c shows examples for recording of fluorescence levels for diploid, Ts65Dn and Tc1 networks respectively. Fig. 1d shows the schematics of the pattern used to measure the velocities. Fig. 1e is a fluorescence image of a neuronal network. The baseline-normalized fluorescence amplitude (see Methods) was reduced in both DS mouse models. This amplitude level was 8.6 ± 0.7% in diploid cultures (N = 12 cultures, n = 227 network bursts) and 5.4 ± 0.3% in Ts65Dn positive cultures (N = 5 cultures, n = 119 network bursts, p = 0.021) (Fig. 1f). For Tc1 negatives (diplod networks) the value was 9.8 ± 0.2% (N = 10 cultures, n = 343 network bursts) compared to 5.1 ± 0.2% (N = 13 cultures, n = 616 network bursts) for Tc1 positive networks ($p < 0.001$) (Fig. 1g). The propagation velocity was also reduced by about 30%, from 160 ± 7 mm/s in diploid networks (N = 12 cultures, n = 227 network bursts) to 108 ± 21 mm/s in Ts65Dn (N = 5 cultures, n = 119 network bursts, p = 0.05) (Fig. 1h), and from 170 ± 8 mm/s in diploid networks (N = 10 cultures, n = 343 network bursts) to 116 ± 3 mm/s in Tc1 (N = 13 cultures, n = 616 network bursts, p = 0.01) (Fig. 1i). In summary, both mouse models exhibit reduced burst amplitudes and propagation velocity in the one-dimensional culture configuration.

3.2. Two-dimensional Trisomic Cultures Have Reduced Network Bursts (Imaging of $[Ca^{2+}]i$)

We next examined if reduced network fluorescence can be detected also in network activity in 2D cultures. Cultures were measured in a range of ages of 12–24 DIV. Network activity usually stabilizes after the first 10–11 DIV. To control for age, for every measurement of Ts65Dn cultures, their littermate diploid cultures were taken in the same DIV.

Fig. 2a shows examples of recorded network bursts of diploid and Ts65Dn networks. The amplitude of the fluorescence signal during activity was smaller in Ts65Dn cultures by about a factor of 2, going from 6.5 ± 1% (N = 12 cultures, n = 266 network bursts) in diploid cultures to 3.3 ± 0.4% in Ts65Dn cultures (N = 10 cultures, n = 253 network bursts, p = 0.014) (Fig. 2b). The average burst duration (see Methods) was also significantly lower (Fig. 2c). We measured 7.1 ± 0.8 s (N = 12 cultures, n = 266 network bursts) in diploid cultures vs. 3.5 ± 0.6 s (N = 10 cultures, n = 253 network bursts) in Ts65Dn cultures (p = 0.0019). To see the contribution of excitatory cells only, we added bicuculline to block $GABA_A$ inhibition, and measured the amplitude of the fluorescence signal (Fig. 2d) giving again a ratio of about 2, with 22 ± 5% (N = 9 cultures, n = 64 network bursts) in diploid cultures versus 9 ± 1.3% (N = 9 cultures, n = 42 network bursts) in Ts65Dn cultures (p = 0.019). Similarly, for the duration of network bursts we measured an average of 2.5 ± 0.3 s (N = 9 cultures, n = 64 network bursts) for the diploid cultures versus 1.8 ± 0.2 s for the Ts65Dn (N = 9 cultures, n = 42 network bursts, p = 0.03) (Fig. 2e). Gradual application of GABA had the effect of reducing network activity until it completely stops. The minimal concentration of GABA needed to stop activity was typically 10 μM to 50 μM depending on how active the culture was. An example is shown in Fig. 2f–i. Fig. 2f shows a recording of the fluorescence signal in a diploid culture with no GABA. Similarly, Fig. 2g shows an example recording for a Ts65Dn culture. Fig. 2h is a recording of the same culture used in Fig. 2f, but with 30 μM GABA application. Fig. 2i similarly shows the Ts65Dn network recording with 30 μM GABA for the same culture used in Fig. 2g. We conclude that network bursts in 2D cultures of the Ts65Dn mouse model were reduced in both amplitude and duration. The ratio of fluorescence amplitudes before and after blocking inhibition is somewhat larger in Ts65Dn, though not statistically significant. This increase may indicate that possible differences in the ratio of excitatory to inhibitory contributions might also play a role.

The reduced network activity observed can be due to increased $GABA_B$ inhibition, which adult Ts65Dn neurons have been shown to have (Créau, 2012; Harashima et al., 2006; Kleschevnikov et al., 2012). To examine this, the $GABA_B$ agonist baclofen was applied at different

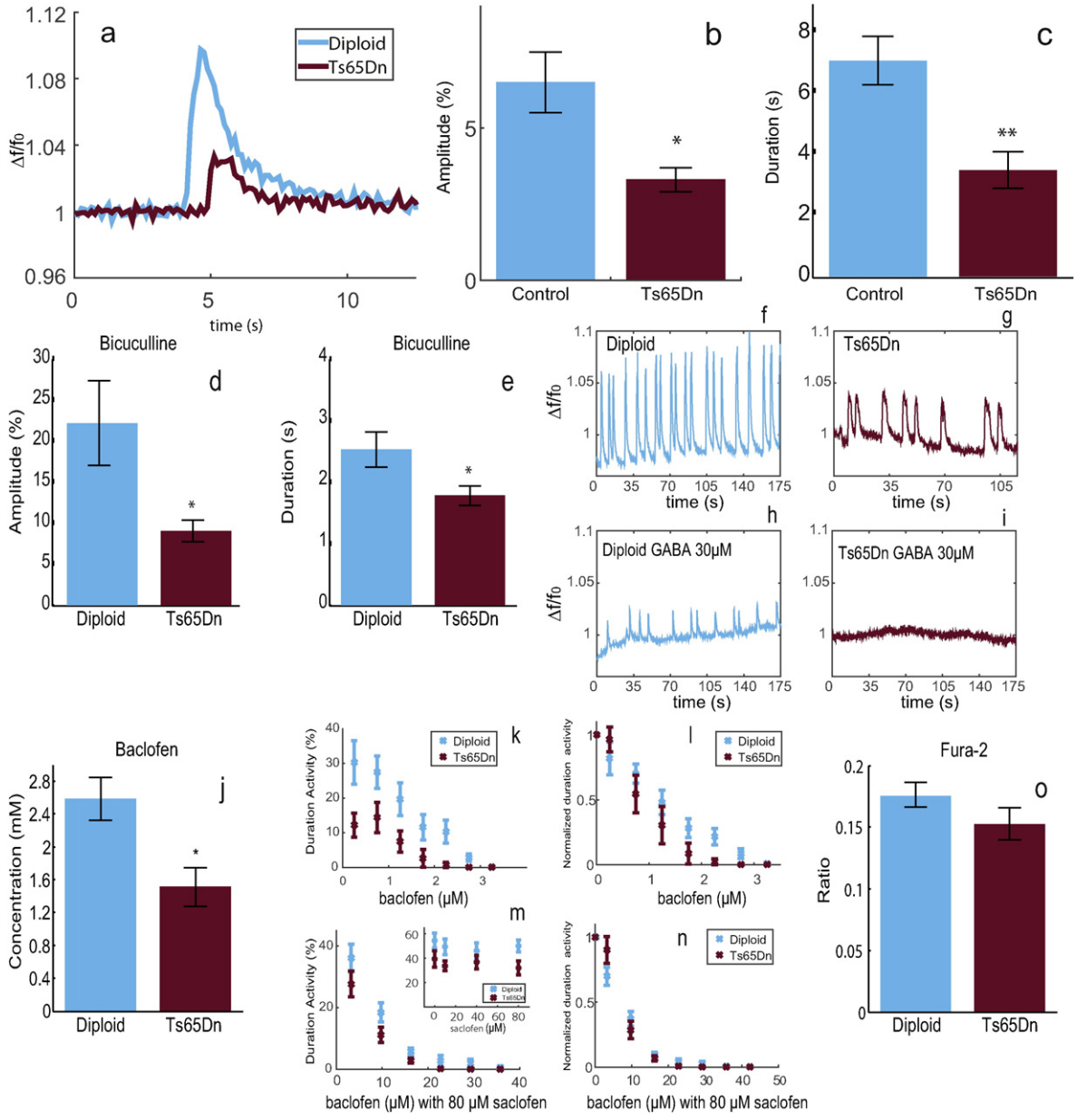

Fig. 2. Analysis of spontaneous network bursts in two-dimensional networks observed by imaging of $[Ca^{2+}]i$. a, Example of time course of the fluorescence intensity ($\frac{\Delta f}{f_0}$) recording of a spontaneous network burst of a two-dimensional diploid vs. Ts65Dn network. b, Amplitude ($\frac{\Delta f}{f_0}$) of diploid networks (N = 8 cultures) vs. Ts65Dn networks (N = 6 cultures), p = 0.014. c, Mean duration of a burst (see Methods for a definition of the duration) of diploid networks (N = 8 cultures) vs. Ts65Dn networks (N = 6 cultures), p = 0.0019. d, Mean normalized fluorescence ($\frac{\Delta f}{f_0}$) intensity of diploid networks (N = 8 cultures) vs. Ts65Dn networks (N = 6 cultures) with inhibitory activity blocked by 40 μM bicuculline, p = 0.019. e, Mean FWHM duration of a burst (see Methods) of diploid networks (N = 8 cultures) vs. Ts65Dn networks (N = 6 cultures) with 40 μM bicuculline, p = 0.03. f, Example of time course for the fluorescence signal of a diploid culture. g, Example of time course for the fluorescence signal of a Ts65Dn culture. h, Same diploid culture as in f, but with 30 μM of GABA applied. i, Same Ts65Dn culture as in f, but with 30 μM of GABA applied. j, Mean baclofen concentration required to stop network activity in diploid networks (N = 5 cultures) vs. the concentration needed to stop activity in Ts65Dn networks (N = 6 cultures), p = 0.0135. k–n, Inhibition plots for baclofen. k, Inhibition plot showing the duration of time that the network was active bursting divided by the total recording time for diploid and Ts65Dn cultures as a function of the baclofen concentration. l, Inhibition plot showing the duration of time that the network was active normalized by the duration of time that the network was active at 0 baclofen for diploid and Ts65Dn cultures as a function of the baclofen concentration. m, Inhibition plot showing the duration that the network was active divided by the total recording time for diploid and Ts65Dn cultures with 80 μM saclofen in the recording medium, as a function of the baclofen concentration. Inset graph shows duration of activity divided by the total recording time as a function of the concentration of saclofen applied. n, Inhibition plot showing the duration that the network was active normalized by the duration that the network was active at 0 baclofen for diploid and Ts65Dn cultures at 80 μM saclofen, as a function of the baclofen concentration. o, Fura-2 ratio of the baseline fluorescent signal at 340 nm to 380 nm in diploid networks (N = 7 cultures) vs. that in Ts65Dn networks (N = 7 cultures), p = 0.185. For panels b–e and j–o data are presented as mean ± SEM, * indicates p-value < 0.05, ** is p < 0.01, and *** indicates p < 0.001.

concentrations, and the stage at which network activity stops was measured. The concentration needed for blocking activity was indeed significantly higher in diploid cultures 2.58 ± 0.26 μM (N = 5 cultures) versus 1.51 ± 0.24 μM (N = 6 cultures) in Ts65Dn (p = 0.0135), as is shown graphically in Fig. 2j. The inhibition plot of baclofen is presented in Fig. 2k, where the total fraction of time that the network was active is shown as a function of the baclofen concentration. In Fig. 2l we normalize the duration that the network was active by the duration of activity at 0 baclofen.

To be certain that activity of baclofen indeed targets the $GABA_B$ receptors, we used saclofen, the $GABA_B$ receptor antagonist, and repeated the baclofen inhibition measurements. In Fig. 2m and n the same inhibition plots as in Fig. 2k and l are given, but with an initial application of 80 μM saclofen. It is clear from these graphs that the baclofen inhibition

plots are considerably shifted to the right with application of saclofen, indicating that these two compounds target the same receptors but with an opposite effect. The inset in Fig. 2m describes the fraction of activity (in %) as a function of the saclofen concentration but with no baclofen, showing that saclofen alone does not have a significant effect. This verifies that $GABA_B$ plays a role in the reduced network activity in the Ts65Dn cultures.

To validate that the reduced fluorescence signal in trisomic cultures did not result from different intracellular calcium levels and reduced uptake of the dye, ratiometric Fura-2 dye was used to quantify the basal level of intracellular calcium. We compared the averaged ratio to illumination at 340/380 nm measured in trisomic cells to that measured in the diploid cells (Fig. 2o). There was no significant difference in Fura-2 ratios between diploid (N = 7 cultures) and Ts65Dn (N = 7 cultures) cultures, with a ratio of 0.17 ± 0.01 in diploid cultures and a ratio of 0.15 ± 0.01 in Ts65Dn ($p = 0.185$). This indicates that basal $[Ca^{2+}]i$ is about the same in the two culture types.

3.3. Electrophysiology in Two-dimensional Cultures Also Reveals Reduced Network Activity

Electrophysiological measurements were used to look for mechanisms that can cause the sharply reduced network activity observed using imaging of $[Ca^{2+}]i$.

3.4. Ts65Dn Networks

Network activity was measured in individual neurons clamped at −60 mV in cultures aged 10 to 15 DIV (Fig. 3). Fig. 3a and c shows examples of an 80 s recording interval of network activity from diploid and Ts65Dn cultures respectively, with a zoom-in on the first 8 s of recording given in Fig. 3b and d respectively. Fig. 3e and f shows the mean burst duration at different days of measurement, while Fig. 3g and h shows for the same days the amount of time that the culture spent bursting (with respect to the total recording time). For young cultures (10–11 DIV), the network activity was similar in Ts65Dn (N = 9 cells) and in diploid cultures (N = 11 cells) (Fig. 3e and g), but for cultures of age > 12 DIV, the diploid cultures had more and longer bursts than Ts65Dn cultures (Fig. 3f and h). Fig. 3f shows that after 12 DIV the mean burst duration for the diploid cultures was 3.03 ± 0.56 s (N = 11 cells), versus 1.34 ± 0.16 s for the Ts65Dn (N = 15 cells, $p = 0.009$). Fig. 3h shows that after 12 DIV diploid networks were more active: they spent 38.3 ± 5.5% (N = 11 cells) of the time bursting while Ts65Dn neurons spent only 9.9 ± 1.7% (N = 15 cells) of the time in bursts ($p < 0.001$).

Young cultures have a rather simple and less connected network structure, and thus their network bursts are shorter in general. In older cultures, there are more connections leading to more complex network activity. We suspect that although the network is more

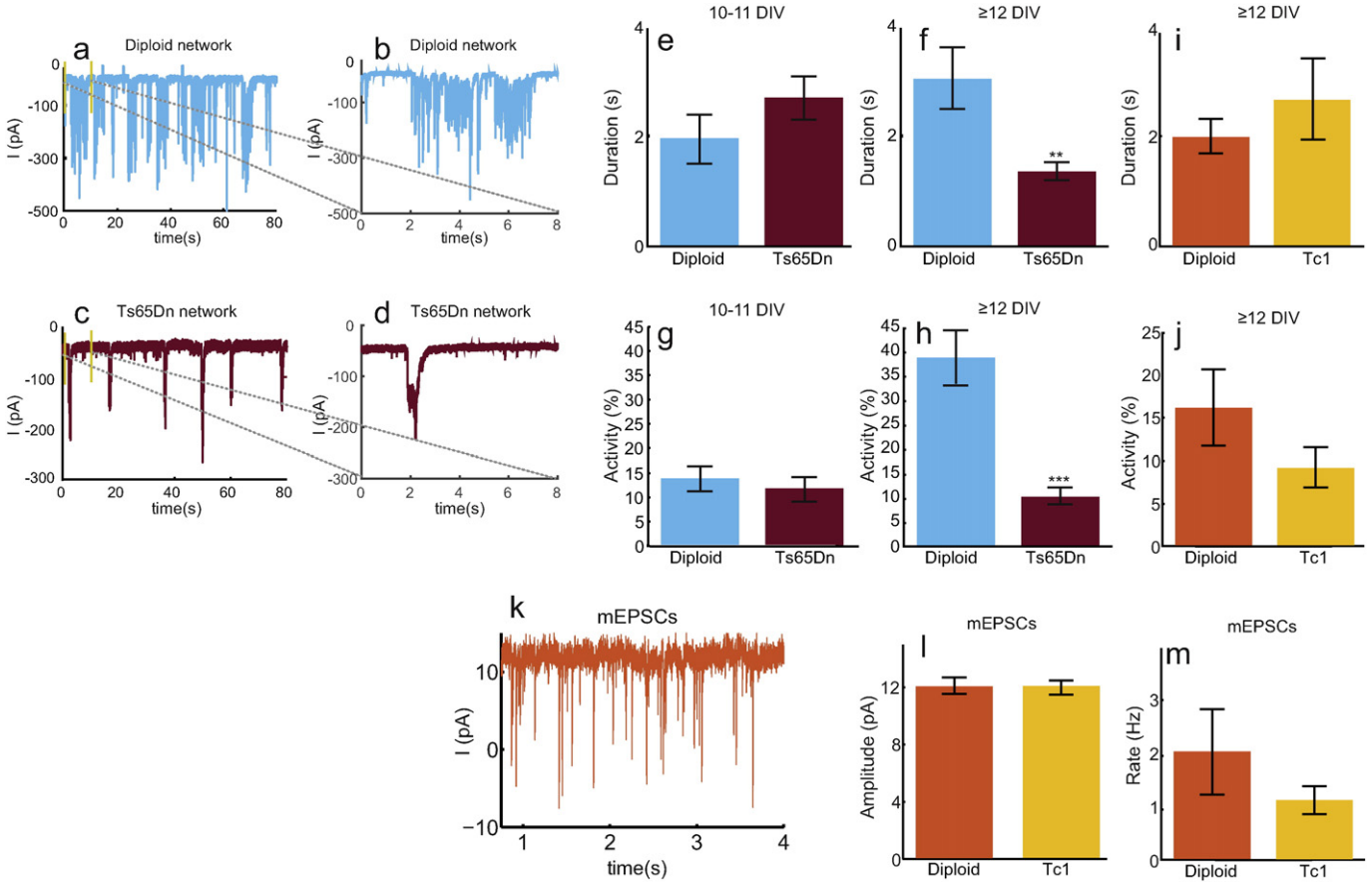

Fig. 3. Analysis of spontaneous network bursts and miniature EPSCs measured with whole cell patch clamp. a, Example of currents recorded during network burst activity for a diploid network (DIV > 12). b, A zoom in on the example recording of the diploid network shown in a. c, Example of currents recorded as in a, for a Ts65Dn network (DIV > 12). d, A zoom in on the example recording of the Ts65Dn network shown in c. e, Mean burst duration for cultures aged 10–11 DIV (diploid N = 11 cells, Ts65Dn N = 9 cells). f, Mean burst duration as in e, but for cultures with ages larger than 12 DIV, (diploid N = 11 cells, Ts65Dn N = 15 cells), $p = 0.009$. g, Total mean bursting time out of total recording time for cultures of ages 10–11 DIV (diploid N = 11 cells, Ts65Dn N = 9 cells). h, Total bursting time out of total recording time for cultures with ages larger than 12 DIV (diploid N = 11 cells, Ts65Dn N = 15 cells), $p = 0.001$. i, Mean burst duration for cultures with ages larger than 12 DIV (diploid N = 20 cells, Tc1 N = 21 cells). j, Total bursting time out of total recording time for cultures with ages larger than 12 DIV (diploid N = 20 cells, Tc1 N = 21 cells), $p = 0.17$. k, Example recording of mEPSCs recorded in the presence of TTX. Note the change in the scale of the y-axis from a and c. l, Mean recorded amplitude of mEPSCs (diploid N = 24 cells, Tc1 N = 29 cells). m, Mean mEPSCs frequency (diploid N = 24 cells, Tc1 N = 29 cells). For panels e–j and l–m results are given as mean ± SEM. * indicates p-value < 0.05, ** is $p < 0.01$, and *** indicates $p < 0.001$.

connected in older Ts65Dn cultures, the lower intrinsic excitability and higher inhibition cause the bursts to remain short.

3.5. Tc1 Networks

Network activity was recorded while holding the cells at −60 mV in cultures aged 12 to 17 DIV (Fig. 3i and j). There was no difference in the burst duration. For the amount of activity there was a slight difference, but not significant: diploid networks spent 16 ± 4% (N = 20 cells) of the time in a burst, whole Tc1 cells spent 9 ± 2% (N = 21 cells) of the time bursting (Fig. 3j, p = 0.17). It is possible that Tc1 cultures have a less pronounced phenotype of reduced network activity because they are mosaic, i.e. Tc1 cultures are a combination of both trisomic and normal cells.

3.6. Tc1 mEPSCs

Miniature Excitatory Post Synaptic Currents (mEPSCs) were measured in the presence of 0.5 μM TTX, while holding the cell at −60 mV. Generally the amount of mEPSCs is highly dependent on the age of the culture, with practically no mEPSCs observed in cultures younger than 13 DIV. We thus measured only for DIV ≥ 13, and in a very low range of ages of the cultures. No differences were found in the average mEPSCs amplitude (N = 24 diploid cells, average age of cultures = 14.7 ± 0.3 DIV, N = 29 Tc1 cells, average age of cultures = 14.3 ± 0.3, see Fig. 3l), and no significant difference was found in the mEPSCs rate (N = 24 diploid cells, N = 29 Tc1 cells, see Fig. 3m). An example of such a recording is shown in Fig. 3k.

3.7. Action Potential Properties Are Different in Ts65Dn and Tc1 Cells

Analysis was performed in current clamp mode using the minimal injected current needed for evoking an action potential. Action potential parameters were analyzed (see Methods for parameter definitions) and are summarized in Table 1. Fig. 4a–c shows examples of action potentials from diploid cells (Fig. 4a) and the two DS models (Fig. 4b and c). Fig. 4a includes a schematic description of some measured parameters, superimposed on the diploid action potential.

A total of 13 diploid cells and 11 Ts65Dn cells were measured. For the Tc1 model a total of 9 diploid cells and 12 Tc1 cells were measured. An increase of about 15% in action potential amplitude for trisomic cells was found in both mouse models. The threshold for evoking an action potential was lower for both DS models by about 4 mV. The input conductance was significantly higher for trisomic cells in both mouse models (~60% Ts65Dn, ~85% Tc1). A striking difference was observed in the 5 ms after hyperpolarization (AHP) amplitude, which was reduced significantly for both mouse models (~75% Ts65Dn, ~50% Tc1). No statistically significant difference was observed for the rise time, resting membrane potential or the decay time (Table 1).

3.8. Number of Action Potentials Produced in Response to Current Injection is Reduced in Ts65Dn and Tc1 Cells

The number of action potentials produced by neurons that were held at different current steps was measured in a time period of 300 ms, as shown in Fig. 4d–h. Fig. 4d and e shows examples of the membrane potential as a function of time at different current steps for a diploid and a Tc1 neuron respectively. Fig. 4f compares the number of action potentials S versus the holding current I for diploid neurons (N = 9 cells) and Ts65Dn model neurons (N = 6 cells). Fig. 4g shows the same analysis for diploid neurons (N = 11 cells) and for Tc1 neurons (N = 9 cells). We analyzed the statistics using a regression comparison (aoctool in Matlab) as explained in the Methods section. The group values were different (p = 0.003) for the Ts65Dn curve and for the Tc1 curve (p = 0.0002). Ts65Dn and Tc1 neurons thus both produced at each 20 pA depolarization step about 1 action potential less per 300 ms recording than the diploid neurons did.

3.9. Fast and Slow Potassium Currents Are Reduced in Ts65Dn and Tc1 Cells

The changes in action potential amplitude, AHP amplitude and spike threshold observed in both DS mouse models point to reduced potassium currents. Potassium currents were then measured in cultured Ts65Dn and Tc1 hippocampal neurons under voltage clamp while blocking sodium currents with TTX. The slow and fast components of the potassium currents were measured (see Methods), and were found to be significantly smaller in both DS mouse model neurons compared to diploids. An example of a recording of potassium currents is shown in Fig. 5a and b. The fast current is also displayed on the small upper inset of these figures, zooming in on the first few milliseconds of recording. The lower inset shows a recording with 4A-P applied at 2 mM. As can be seen the fast currents are eliminated, indicating that these are mainly A-type potassium currents. A total of 23 diploid neurons and 27 Ts65Dn neurons were measured, and their results are

Table 1
Action potential parameters of Ts65Dn, Tc1 vs. diploid neurons. and of simulated DS neurons vs. WT neurons.

Experiment	Diploid (N = 13)	Ts65Dn (N = 11)	P value	Ratio (diploid/Ts65Dn)
Action potential amplitude (mv)	66.7 ± 2.5	78.4 ± 2.4	0.0027	0.85 ± 0.04
Rise time (ms)	0.75 ± 0.05	0.69 ± 0.04	0.34 (N.S.)	1.09 ± 0.1
5 ms AHP (mV)	−11 ± 2	−2.7 ± 0.6	0.0016	4.1 ± 1.1
Threshold (mV)	−27.1 ± 1.2	−30.5 ± 0.7	0.0282	0.89 ± 0.044
Input conductance (nS)	3.3 ± 0.4	5.3 ± 0.5	0.0045	0.62 ± 0.1
Resting membrane potential (mV)	−56.8 ± 1.8	−53.3 ± 1.3	0.19 (N.S.)	1.07 ± 0.04
Experiment	Diploid (N = 9)	Tc1 (N = 12)	P value	Ratio (Diploid/Tc1)
Action potential amplitude (mV)	64.5 ± 1.5	76.6 ± 1.4	1.7e-5	0.84 ± 0.03
Rise time (ms)	0.96 ± 0.13	0.94 ± 0.06	0.89 (N.S.)	1.02 ± 0.15
5 ms AHP (mV)	−7 ± 1.1	−3.4 ± 0.6	0.02	2.05 ± 0.48
Threshold (mV)	−26.3 ± 1.3	−30.8 ± 1	0.02	0.85 ± 0.05
Input conductance (nS)	2.8 ± 0.3	5.2 ± 0.6	0.01	0.54 ± 0.09
Resting membrane potential (mV)	−60.3 ± 1.9	−58.8 ± 3.4	0.71 (N.S.)	1.03 ± 0.07
Simulation	WT	DS		Ratio (WT/DS)
Action potential amplitude (mV)	64.7	66.4		0.97
AHP (mV)	12	7.6		1.58
Threshold (mV)	−49	−50		0.98
Input conductance (S/m^2)	2.05	2.54		0.81
Resting membrane potential	−74.7	−73.5		1.02

The parameters are defined in the Methods section. N.S. = not significant.

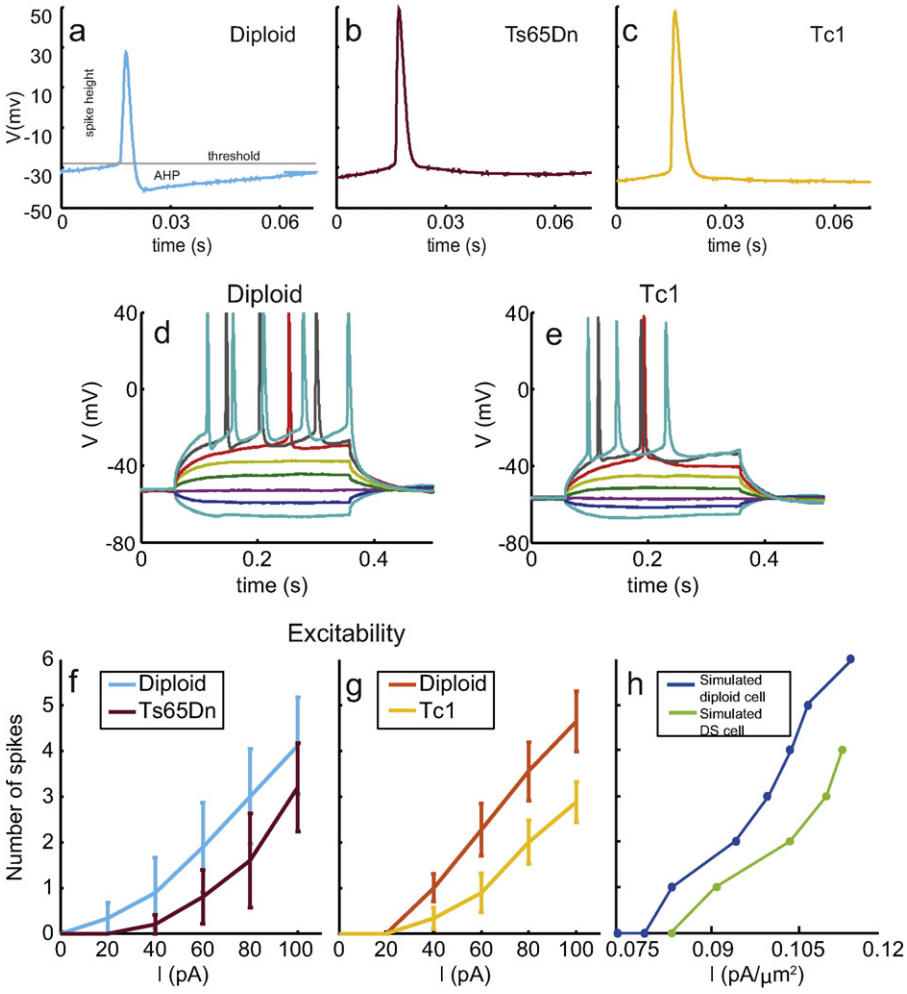

Fig. 4. Action potentials recorded in current clamp. a, Example of the time course of the membrane potential during spiking in a diploid neuron. Schematics of some of the parameters analyzed are superimposed on the action potential. The gray line designates the value of the threshold voltage. b, A similar example for a Ts65Dn neuron c, A similar example for a Tc1 neuron. d–h, Number of action potentials per 300 ms at consecutive depolarization current steps (20 pA apart). d, An example of the membrane potential recording for a diploid neuron at different current steps. e, A similar example for a Tc1 neuron. f, Number of action potentials produced vs. injected current for diploid neurons (N = 9 cells) compared to Ts65Dn neurons (N = 6 cells), p = 0.003. g, Number of action potentials produced vs. injected current for diploid neurons (N = 9 cells) compared to Tc1 neurons (N = 12 cells), p = 0.0002. For panels f and g data are given as mean ± SEM. h, Results of the simulation. Shown is the number of action potentials produced in a 300 ms current injection step as a function of the current amplitude, for a simulated diploid cell compared to a simulated DS cell.

plotted in Fig. 5c (fast) and d (slow). Similarly, a total of 36 diploid neurons and 36 Tc1 neurons were measured, and their results are plotted in Fig. 5e (fast) and f (slow).

The effect was more pronounced in the Ts65Dn mice, where the fast and slow current responses at the maximal voltage step were lower by about 35% of the diploid cells. An ANOVA test performed using aoctool in Matlab shows that the two curves for both the fast and slow potassium currents are statistically different ($p = 0.0004$, $p = 0.008$ respectively). In the Tc1 mice the effect was smaller, where a reduction of about 25% from the diploid cell values were measured for the fast currents and a reduction of about 15% was measured for the slow current components. An ANOVA test performed using aoctool in Matlab shows that the two curves for both the fast and slow potassium currents are statistically different ($p = 0.0021$, $p = 0.082$ respectively)

3.10. Numerical Simulation

To reproduce numerically the measured changes in the action potential shape, the reduced excitability and reduced potassium currents, a WT versus a DS neuron were simulated. The main drive for the simulation was that our two main results seem to contradict each other: a cell which has reduced potassium currents should be more excitable. Our DS neurons, on the contrary, have reduced potassium currents yet are less excitable.

The simulated neuron was spatially extended according to the model by Migliore (2012) and Migliore and Migliore (2012), and its dynamics were prescribed by a combination of one sodium channel, one cation and four different potassium channels (see Methods). DS differed from WT cells in the values of the conductance of the cation and potassium channels, which were chosen to yield behavior similar to the experimental results. The values chosen for WT versus DS conductance are given in Table 2.

The effect of changes in channel conductance in the simulation was different for each channel. Reduced conductance of the delayed rectifier caused a concurrent reduction in the AHP, in line with previous work (Lorenzon and Foehring, 1992). It did not affect excitability. Reduced A-type potassium channel conductance reduced the AHP, similar to the effect reported in Giese et al. (1998). It also had an additional effect of increasing the cell excitability, and this effect was also previously reported (Shibata et al., 2000). Increased HCN channel conductance reduced cell excitability, raised the resting membrane potential and had almost no effect on the fast or slow potassium currents. It has been

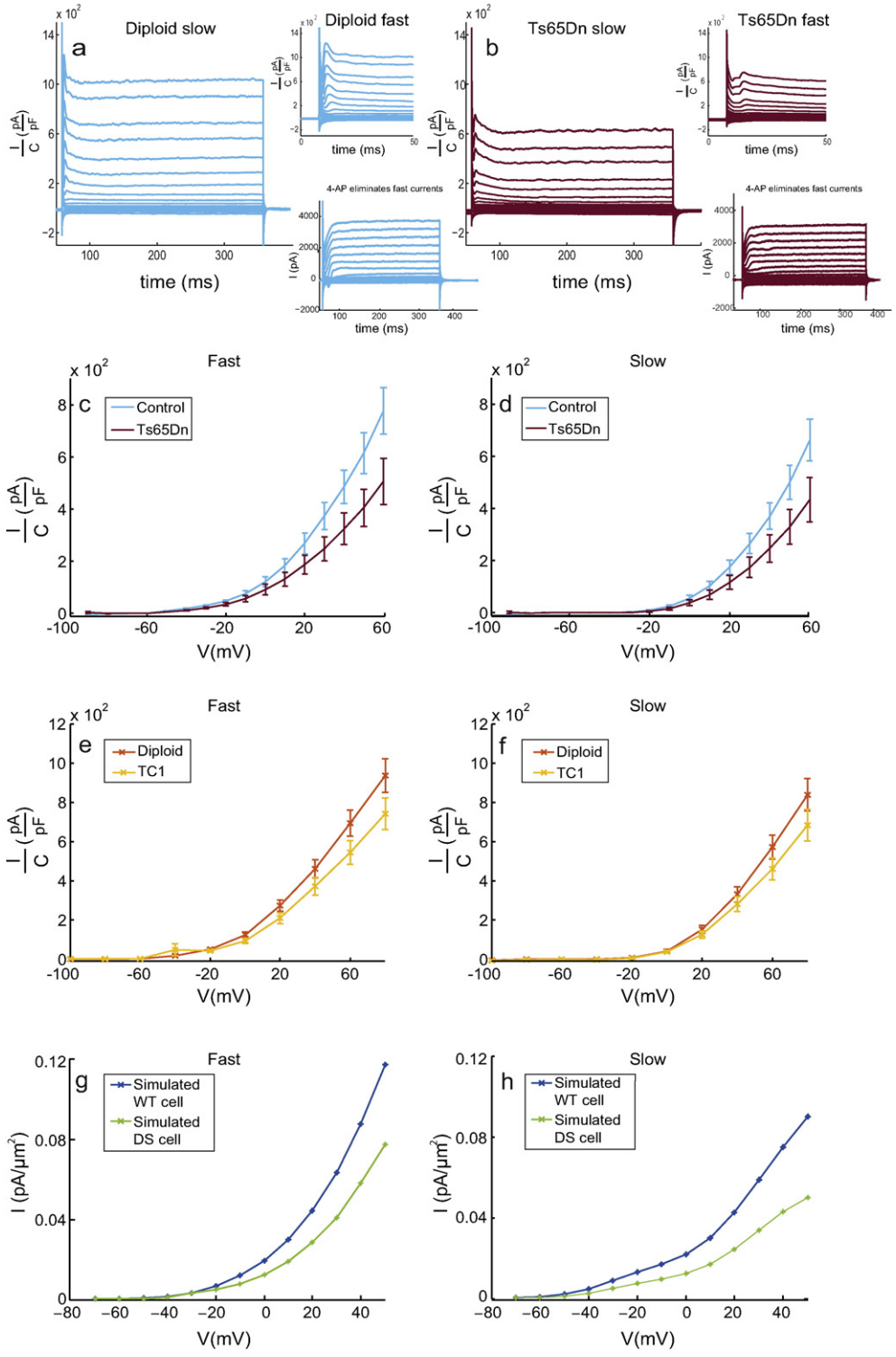

Fig. 5. Experimental measurement and numerical simulation of potassium currents. a–f, Experimental results under voltage clamp with voltage steps going from −90 mV to 80 mV. The currents are normalized by the estimated capacitance of the cell (see Methods). Fast currents are measured as the peak current a few milliseconds after the depolarization step. Slow currents are measured towards the end of the depolarizing step, which occurs 300 ms after its beginning. a, Example recording of potassium currents for a diploid cell. The current is normalized by the capacitance of the cell. Top inset: Zooming in on the first 50 ms of recording, the fast currents can be observed as the peak current a few milliseconds after the voltage step. Bottom inset: Fast currents are eliminated by application of 2 mM 4-aminopyridine indicating that they are mostly A-type potassium currents. b, Example recording of potassium currents for a Ts65Dn cell. The current is normalized by the capacitance of the cell. Top inset: Zooming in on the first 50 ms of recording, the fast currents can be observed as the peak current a few milliseconds after the voltage step. Bottom inset: Fast currents are eliminated by application of 2 mM 4-aminopyridine indicating that they are mostly A-type potassium currents. c, Fast potassium currents of diploid neurons (N = 23 cells) are larger compared to Ts65Dn neurons (N = 27 cells), p = 0.0004. d, Slow potassium currents of diploid neurons (N = 23 cells) are larger compared to Ts65Dn neurons (N = 27 cells), p = 0.008. e, Fast potassium currents of diploid neurons (N = 36 cells) are larger compared to Tc1 neurons (N = 36 cells), p = 0.0021. f, Slow potassium currents of diploid neurons (N = 36 cells) are larger compared to Tc1 neurons (N = 36 cells), p = 0.082. For panels c–f data are presented as mean ± SEM. g, h, Simulation results. g, The fast potassium currents measured in simulated DS cells compared to those measured in WT cells. h, Simulated slow potassium currents in DS cells compared to WT cells.

Table 2
Values of the channel conductances used as parameters to describe WT and DS cells in the numerical simulation.

	Sodium	Delayed rectifier	A-type	HCN	m-Channels	Inward rectifiers
Healthy	0.015	0.007	0.06	0.0004	0.0023	0.004
DS	0.015	0.0033	0.033	0.0007	0.0013	0.007

All values are given in units of mS/cm^2.

shown that increased h-currents (associated with HCN channels) reduce the cell excitability and raise resting membrane potential (Li et al., 2012). Reduction in M-channel conductance increased cell excitability, in line with previous reports in Peretz et al. (2005) and reduced slow potassium currents. Increased inward rectifier conductance lowered the resting membrane potential and lowered the cell excitability (though this is a weak effect), consistent with the literature (Doupnik et al., 1995).

A comparison between the action potential parameters of the simulated WT cell and those of the simulated DS cell is given in Table 1. A graph of the action potential shape for the WT and the DS cell is given in the Supplementary Material, Fig. S1. Fig. 4h shows the excitability of the simulated neurons, which was measured numerically for varying stimulation current steps. DS cells showed reduced excitability compared to WT cells, with about one action potential less per depolarization step. The fast and slow potassium currents were also calculated numerically as a function of increased stimulation voltage, as plotted in Fig. 5g and h respectively. Comparison with the experimental data in Table 1 and in Figs. 4 and 5 shows that the simulation qualitatively reproduces the action potential shape, and captures the reduction in potassium currents and excitability to a quantitative agreement with the experiment. Moreover the simulation shows that the coexistence of reduced potassium currents with reduced excitability in DS cells is due to a balance of reduced outward rectifying potassium channels and increased inwardly rectifying and HCN channels.

The model shows that a suitable combination of changes in channel conductance can account for the measured results, but it also predicts specifically that the A-type, delayed and inward rectifiers, M-type and HCN channels should all be modified in the cell. To validate the prediction of the model, we thus examined all these currents.

3.11. A-type and Delayed Rectifier Potassium Currents Are Reduced in Ts65Dn and Tc1 Cells

The reduction in the activity of the A-type and the delayed rectifier is actually already evident in the traces and results of Fig. 5, where the slow and fast potassium currents are reported. The slow component is known to be related to the delayed rectifier (Huguenard et al., 1991), and is reduced by about 35% in the Ts65Dn and about 15% in the Tc1 models. The fast potassium current reported in Fig. 5 is associated with the A-type channels (Huguenard et al., 1991; Yuan et al., 2005), and as shown in the lower inset of Fig. 5a and b, is indeed blocked by 4-AP, which at these concentrations mainly blocks the A-type channel.

3.12. Inward Rectifying Potassium Channels Are Over-expressed in Ts65Dn Cells

The inward rectifier KCNJ6 has been shown by others to be overexpressed (Harashima et al., 2006). We measured expression levels of the inward rectifying potassium channel KCNJ15 in hippocampus tissue of Ts65Dn mice using quantitative RT-PCR, and observed a fold change of 1.4 (40% increase) in the expression level in Ts65Dn ($p = 0.014$ $N = 20$ diploid pups and $N = 19$ Ts65Dn pups). Tables summarizing the data for the embryos/pups analyzed are given in the Supplementary Material.

3.13. M-type Potassium Currents Are Reduced in Ts65Dn Cells

M-type currents were measured under whole cell patch clamp in voltage clamp mode in Ts65Dn cultured neurons by comparing currents with and without linopirdine in the presence of TTX and Cesium. The effect of linopirdine on the current is shown for diploid cells (Fig. 6a) and for Ts65Dn cells (Fig. 6b). M-type currents were significantly lower in Ts65Dn cells compared to diploids, as shown in Fig. 6c. Average M-type currents for diploid cells were 25 ± 7 pA ($N = 32$ cells) and a strikingly low value of 2 ± 5 pA ($N = 25$ cells) for Ts65Dn cells ($p = 0.017$), so that there were almost no M-type currents in Ts65Dn cells.

3.14. HCN Sag is Increased in Ts65Dn Cells

HCN sag was measured in whole cell patch clamp in current clamp mode in Ts65Dn cultured neurons vs. diploid neurons. The cell was hyperpolarized to ~− 100 mV for 1 s, and the voltage sag was measured by the difference between the minimal current, typically attained after 200 ms, and the level reached just before 1 s (see Methods). An example recording for a diploid cell and a Ts65Dn cell is shown in Fig. 6d. This sag is known to be proportional to the HCN current (Angelo and Margrie, 2011) and it is blocked by Cesium, as can be seen in Fig. 6e, indicating that it is due to HCN currents. On average, diploid cells had a sag of 4.2 ± 0.5 mV ($N = 30$ cells) while Ts65Dn cells had a significantly larger sag of 6.9 ± 0.8 ($N = 27$ cells, $p = 0.0044$).

After measuring the relevant currents we went back to the model, and verified that the measured values for the M-type and HCN channels can very well be incorporated in the model, with little changes to the other channels needed to maintain the phenotype very close to what the model previously gave.

4. Discussion

We have presented evidence that DS model trisomic neurons behave differently than diploid neurons, at both the cellular and the network levels. Our findings point to five mechanisms that may be implicated in the pathology of DS. The first two are an increase in inward rectification and HCN currents, causing the cells to be less excitable. The other three are reduced A-type, delayed rectifier and M-type potassium currents. Differences were found in the action potential shape, in particular a sharp reduction in the AHP amplitude, but also a rise in action potential amplitude, a lower threshold for spiking and a higher input conductance. Both Ts65Dn and Tc1 models exhibited similar changes from diploid cells, confirming the robustness of the measurements, with some differences between the models. The Ts65Dn mice showed a more pronounced effect in the main results of reduced potassium currents and smaller AHP. This may be due to the fact that the Tc1 are mosaic, so that some Tc1 neurons that were examined may have been normal cells.

The reduced outward potassium currents are evident in a number of measurements. Indirect evidence for this reduction is in the action potential properties, showing that in trisomic cells the amplitude of the action potential is higher, the threshold for excitation is lower and the AHP amplitude is sharply reduced (Fig. 4 and Table 1). Direct measurement giving voltage depolarization steps showed reduced potassium currents at all voltage steps (Fig. 5). The fast potassium currents we measured are known to be mainly A-type currents (Huguenard et al., 1991; Yuan et al., 2005). We also applied 4-AP and observed how these currents were blocked (Fig. 5a and b Inset). The slow potassium currents were shown to be mainly delayed rectifier currents (Huguenard et al., 1991).

The reduced excitability is also evident in several measurements, mostly related to network activity. Imaging of $[Ca^{2+}]i$, we observed that the fluorescence amplitudes and the duration of network bursts in 2D cultures were reduced (Fig. 2). This network bursting activity was suppressed by lower concentrations of baclofen in Ts65Dn

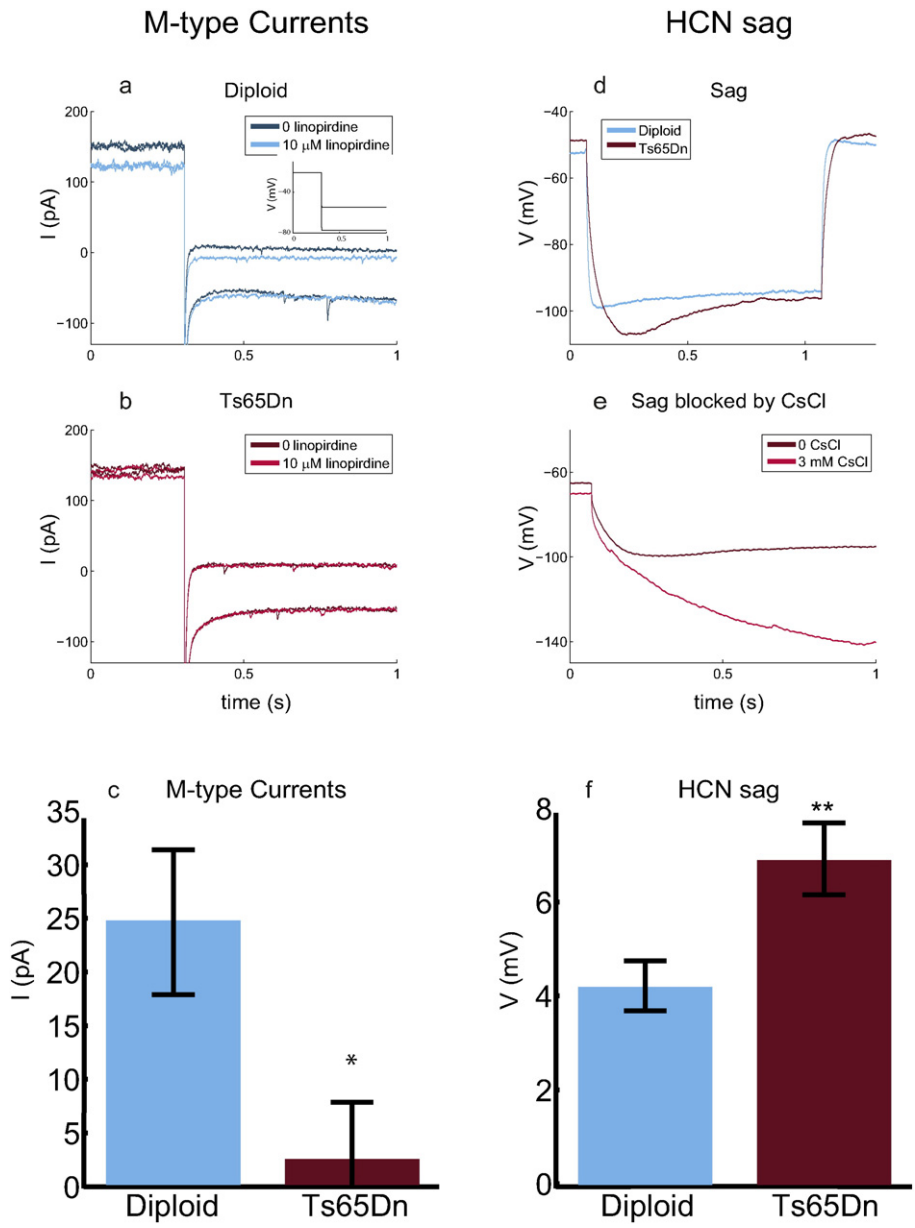

Fig. 6. M-type and HCN currents. a, An example of the current recorded from a diploid cell with (light line) and without (dark line) linopirdine in voltage clamp. Inset: Voltages used to clamp the cell. b, A similar example for a Ts65Dn neuron. This example displays almost no M-type current. c, Mean M-type currents for diploid (N = 32 cells) and Ts65Dn cells (N = 25 cells), p = 0.017. d, An example of the HCN voltage sag in current clamp for a diploid cell versus a Ts65Dn cell. e, Application of CsCl (3 mM) completely eliminates the voltage sag, shown in an example of a TS65Dn cell. f, Mean HCN voltage sag for diploid cells (N = 30 cells) versus Ts65Dn cells (N = 27 cells), p = 0.0044. For panels c and f data are presented as mean ± SEM, * indicates p-value < 0.05, ** is p < 0.01.

networks than in diploid networks, pointing to increased $GABA_B$ inhibition (Fig. 2j). The propagation of bursting activity in one-dimensional linear networks is furthermore slower and weaker in Ts65dn and Tc1 cultures versus those of diploid cultures (Fig. 1). Finally, the network activity of Ts65Dn networks measured using electrophysiology, while holding the cells at −60 mV, also showed decreased burst duration and reduced overall bursting activity (Fig. 3f and h). At the single cell level we found that neurons in both DS mouse models produced fewer action potentials in a given measured time for repetitive spiking at all current steps in which action potentials appeared (Fig. 4). We also measured increased input conductance in both DS mouse models. The large increase in input conductance causes a large decrease in cell excitability and is a combination of two factors: increased HCN currents and increased inward rectifying currents. These two changes also balance the resting membrane potential: inward rectifiers are known to lower the resting membrane potential (Reimann and Ashcroft, 1999) and HCN channels are known to raise it, because their reversal potential is high (Biel et al., 2009). The overall effect is a slight rise of the resting membrane potential in both DS models and also in the model (Table 1).

The reduced excitability can be cell intrinsic, i.e. due to increased inward rectification and increased HCN currents, but it may also be due to weaker synapses: smaller and less frequent mEPSCs were measured in organotypic and acute slices by Hanson et al. (2007) for the Ts65Dn model. On the other hand Best et al. (2008) reported no difference of mEPSCs frequency or amplitude in cultures of Ts65Dn. We measured mEPSCs for Tc1 neurons and did not observe a difference in amplitude. The rate of mEPSCs was reduced, but not significantly. Since we

measured reduced excitability also at the cell level (Fig. 4), and since the increase in input conductance we observed is also a major factor in cell excitability, weaker synapses could contribute to reduced excitability, but the intrinsic properties of the cell, increased inward rectification and increased HCN currents, probably play a major role.

Our numerical simulation demonstrates that the DS phenotype can be reproduced by changing the conductance of the delayed rectifier, inward rectifier, HCN, M-type and A-type channels. These modifications also combine to give an action potential shape that is similar to the experimentally observed one (reduced AHP, increased action potential amplitude and reduced threshold for spiking). The simulation points at the delayed rectifiers, the A-type channels and the M-type channels as leading to the reduced potassium currents. The delayed rectifiers and the A-type channels are less active in DS, and their effect is to decrease the fast potassium currents and to reduce AHP amplitude. The reduction in slow currents is dominated by the decreased activity of M-type channels and delayed rectifier channels. At the same time, the simulation indicates that the reduction in the conductance of A-type channels and in the M-type channels can contribute to an increased excitability, an effect which is countered by the increase in the conductance of the inward rectifying and HCN channels. Thus the overall behavior is a balance of all these changes and effects, which successfully reproduces the experimental observation of decreased outward potassium currents and reduced excitability at the same time.

Our simulation of a DS cell used five different mechanisms. DS cells exhibited an increase of inhibition caused by increased conductance of the inward rectifying potassium currents. The G-coupled inward rectifier KCNJ6 was already shown to be overexpressed by Quantitative RT-PCR by Harashima et al. (2006), and indeed, we have found that KCNJ15, another inward rectifying potassium channel on the Down Syndrome Critical Region (DSCR), is also overexpressed in hippocampal tissue of Ts65Dn embryos. We went on to measure the other two types of channels, which were predicted by the model to have altered conductance: HCN and M-type potassium currents. Using whole cell patch clamp, we have shown that Ts65Dn cells had a sharp decrease of about 90% in the M-type currents. We have also shown with electrophysiology, that the HCN currents are increased by about 65% in Ts65Dn cells compared to diploid cells. As for the A-type and delayed rectifier that are also included in the simulation, they are directly related to the fast and slow currents that we measured.

Reduced potassium currents were not previously reported at all in DS mouse model cells, but clues to their existence can be found in several studies. An indirect observation is that Ts65Dn mice are hyperactive and have tremor convulsions (Davisson et al., 1993; Sago et al., 2000), a form of behavioral hyperactivity that can be linked with reduced potassium currents (Wulff and Zhorov, 2008). In general, the reduction of potassium currents has been linked to changes in the neuronal action potential structure, to a reduction in AHP amplitude, and possibly to impairment of learning ability (Disterhoft et al., 1996; Giese et al., 1998). In our simulation, we also saw that reduced currents are linked with a decrease in the AHP, since the reduced A-type potassium channels and delayed rectifier channels cause a reduction in the fast potassium currents but at the same time also reduce AHP.

Evidence for reduced AHP in trisomic cells was previously reported by Orozco et al. (1987, 1988), who measured single neuron properties of the old Ts16 DS mouse model Dorsal Root Ganglion (DRG). They found a reduction of 16% in the after hyperpolarization (AHP) amplitude and 42% reduction in its duration along with an increase of about 5 mV in the action potential amplitude with a lower threshold for excitation and an increase in input conductance. Scott et al. (1981) also observed reduced AHP in neurons taken from human fetuses with DS.

Previous work at the single cell level has demonstrated the link between increased $GABA_B$ inhibition and reduced excitability (Best et al., 2007), but here we show that these effects exist also at the network level. Increased HCN currents were not reported previously in DS mouse model cells, but the effect of HCN currents as a possible mechanism for reduced excitability in a wild-type diploid hippocampal cell has been shown by (Albertson (2012) and Li et al. (2012)).

It is interesting to look for analog symptoms in human DS, although it should be kept in mind that both the Ts65Dn and the Tc1 models have features that confound the comparison to human DS. In the Ts65Dn mouse there are only 50% of the DS genes and about 50 genes with copy number gains (Reinholdt et al., 2011). The Tc1 model, on the other hand, has a number of genes with rearrangements and deletions, even in the DSCR (Gribble et al., 2013), and therefore gene differences exist with respect to the extra chromosome of the Ts65Dn mouse model. Such differences are potential confounding factors.

As noted above, reduced AHP was seen in neurons of human fetuses (Scott et al., 1981), who in fact also hypothesized that reduced AHP is linked to reduced potassium currents. Altered and reduced AHP are known to affect learning processes, and may contribute to the cognitive disability in Down syndrome, for example Disterhoft et al. (1996) showed that aging hippocampal neurons have decreased AHP and decreased ability to learn. Another interesting connection between our networks to human DS behavior regards the reduction in the propagation velocity of activity that we report. A reduced velocity of electrical signal propagation was reported in auditory ERPs, in muscle responses and in EEG potentials in people with DS (Vieregge et al., 1992). A possible relation can also be found between the reduction in potassium currents and a higher incidence of hyperactivity and of epilepsy in the DS population (Goldberg-Stern et al., 2001; Arya et al., 2011), since reduced potassium currents can be a cause of epilepsy (Singh et al., 1998) and of hyperactivity (Wulff and Zhorov, 2008).

5. Conclusions

We have provided both experimental and simulation evidence that the observed neuro-pathological traits of a DS mouse model cell can be described by changes in conductance of 5 types of ion channels. A reduction in the outwardly rectifying potassium currents — The A-type, the M-type and the delayed rectifier — is concurrent with the opposite trend of an increase in HCN currents and in the inward rectifier currents. The overall contribution of these changes results in a trsiomic cell with slight changes in action potential shape and with reduced potassium currents, in spite of which it is less excitable, and the neural network it forms is less active. These observations were reproduced in both mouse models and in the numerical simulation.

Conflicts of Interest

Authors declare no conflicts of interest.

Acknowledgments

The authors thank Elizabeth Fisher for supplying the Tc1 mice and for many helpful suggestions and remarks, and Ofer Feinerman, Eitan Reuveny, Yaron Penn, Eyal Weinreb and Renaud Renault for very helpful discussions. We thank Shira Silberberg for the help in the genetic analysis, and Rinat Keren for help in Quantitative RT-PCR analysis. This work was partly supported by the Minerva Foundation (Munich, Germany) and by the Israel Science Foundation grant 1415/12 and the Clore Center for Biological Physics.

Appendix A. Supplementary Data

Supplementary data to this article can be found online at http://dx.doi.org/10.1016/j.ebiom.2015.07.038.

References

Ahmed, M.M., et al., 2013. Protein profiles in Tc1 mice implicate novel pathway perturbations in the Down syndrome brain. Hum. Mol. Genet. 22 (9), 1709–1724 (Available at: http://www.ncbi.nlm.nih.gov/pubmed/23349361).

Akeson, E.C., et al., 2001. Ts65Dn — localization of the translocation breakpoint and trisomic gene content in a mouse model for Down syndrome. Cytogenet. Cell Genet. 93, 270–276.

Albertson, A.J., 2012. Hcn Channels and Regulation of Neocortical Network Activity. Ph.D. Thesis, The University of Alabama at Birmingham.

Angelo, K., Margrie, T.W., 2011. Population diversity and function of hyperpolarization-activated current in olfactory bulb mitral cells. Sci. Rep. 1 (50).

Arya, R., Kabra, M., Gulati, S., 2011. Epilepsy in children with Down syndrome. Epileptic Disord. 13 (1), 1–7.

Aylward, E.H., et al., 1997. Cerebellar volume in adults with Down syndrome. Arch. Neurol. 54, 209–212.

Baxter, L.L., et al., 2000. Discovery and genetic localization of Down syndrome cerebellar phenotypes using the Ts65Dn mouse. Hum. Mol. Genet. 9 (2), 195–202 (Available at: http://www.ncbi.nlm.nih.gov/pubmed/10607830).

Best, T.K., Siarey, R.J., Galdzicki, Z., 2007. Ts65Dn, a mouse model of Down syndrome, exhibits increased GABAB-induced potassium current. J. Neurophysiol. 97 (1), 892–900 (Available at: http://www.ncbi.nlm.nih.gov/pubmed/17093127).

Best, T.K., et al., 2008. Speeding of miniature excitatory post-synaptic currents in Ts65Dn cultured hippocampal neurons. Neurosci. Lett. 438 (3), 356–361 (Available at: http://www.ncbi.nlm.nih.gov/pubmed/18490108).

Best, T.K., et al., 2012. Dysfunctional hippocampal inhibition in the Ts65Dn mouse model of Down syndrome. Exp. Neurol. 233 (2), 749–757.

Biel, M., et al., 2009. Hyperpolarization-activated cation channels: from genes to function. Physiol. Rev. 89 (3), 847–885.

Cramer, N., Galdzicki, Z., 2012. From abnormal hippocampal synaptic plasticity in down syndrome mouse models to cognitive disability in Down syndrome. Neural Plast. 101542 (Available at: http://www.ncbi.nlm.nih.gov/pubmed/22848844).

Créau, N., 2012. Molecular and cellular alterations in Down syndrome: toward the identification of targets for therapeutics. Neural Plast. 2012, 171639.

Davisson, M.T., et al., 1993. Segmental trisomy as a mouse model for Down syndrome. Prog. Clin. Biol. Res. 384, 117–133 (Available at: http://www.ncbi.nlm.nih.gov/pubmed/8115398).

Deidda, G., et al., 2015. Reversing excitatory $GABA_AR$ signaling restores synaptic plasticity and memory in a mouse model of Down syndrome. Nat. Med. 21 (4), 318–326 (Available at: http://dx.doi.org/10.1038/nm.3827).

Demas, G.E., et al., 1996. Spatial memory deficits in segmental trisomic Ts65Dn mice. Behav. Brain Res. 82 (1), 85–92.

Disterhoft, J.F., et al., 1996. Calcium-dependent afterhyperpolarization and learning in young and aging hippocampus. Life Sci. 59 (5–6), 413–420 (Available at: http://www.ncbi.nlm.nih.gov/pubmed/8761329).

Doupnik, C.A., Davidson, N., Lester, H.A., 1995. The inward rectifier potassium channel family. Curr. Opin. Neurobiol. 5 (3), 268–277 (Available at: http://www.ncbi.nlm.nih.gov/pubmed/7580148).

Feinerman, O., Segal, M., Moses, E., 2005. Signal propagation along unidimensional neuronal networks. J. Neurophysiol. 94 (5), 3406–3416 (Available at: http://www.ncbi.nlm.nih.gov/pubmed/16049148).

Garner, C.C., Wetmore, D.Z., 2012. Synaptic pathology of down syndrome. Adv. Exp. Med. Biol. 970, 451–468.

Giese, K.P., et al., 1998. Reduced K+ channel inactivation, spike broadening, and after-hyperpolarization in Kvbeta1.1-deficient mice with impaired learning. Learn. Mem. 5 (4–5), 257–273 (Available at: http://www.ncbi.nlm.nih.gov/pubmed/10454353).

Goldberg-Stern, H., et al., 2001. Seizure frequency and characteristics in children with Down syndrome. Brain Dev. 23 (6), 375–378 (Available at: http://www.ncbi.nlm.nih.gov/pubmed/11578846).

Gribble, S.M., et al., 2013. Massively parallel sequencing reveals the complex structure of an irradiated human chromosome on a mouse background in the Tc1 model of Down syndrome. PLoS One 8 (4), e60482 (Available at: http://www.ncbi.nlm.nih.gov/pubmed/23596509).

Gruber, A.J., et al., 2003. Modulation of striatal single units by expected reward: a spiny neuron model displaying dopamine-induced bistability. J. Neurophysiol. 90 (2), 1095–1114 (Available at: http://www.ncbi.nlm.nih.gov/pubmed/12649314).

Hanson, J.E., et al., 2007. The functional nature of synaptic circuitry is altered in area CA3 of the hippocampus in a mouse model of Down's syndrome. J. Physiol. 579 (Pt 1), 53–67 (Available at: http://www.ncbi.nlm.nih.gov/pubmed/17158177).

Harashima, C., et al., 2006. Abnormal expression of the G-protein-activated inwardly rectifying potassium channel 2 (GIRK2) in hippocampus, frontal cortex, and substantia nigra of Ts65Dn mouse: a model of Down syndrome. J. Comp. Neurol. 494 (5), 815–833 (Available at: http://www.ncbi.nlm.nih.gov/pubmed/16374808).

Hattori, M., et al., 2000. The DNA sequence of human chromosome 21. Nature 405 (6784), 311–319 (Available at: http://www.ncbi.nlm.nih.gov/pubmed/10830953).

Herault, Y., et al., 2012. The in vivo Down syndrome genomic library in mouse. Prog. Brain Res. 197, 169–197.

Hines, M.L., Carnevale, N.T., 1997. The NEURON simulation environment. Neural Comput. 9 (6), 1179–1209 (Available at: http://www.ncbi.nlm.nih.gov/pubmed/9248061).

Huguenard, J.R., Coulter, D.A., Prince, D.A., 1991. A fast transient potassium current in thalamic relay neurons: kinetics of activation and inactivation. J. Neurophysiol. 66, 1304–1315.

Hyde, L.A., Frisone, D.F., Crnic, L.S., 2001. Ts65Dn mice, a model for Down syndrome, have deficits in context discrimination learning suggesting impaired hippocampal function. Behav. Brain Res. 118 (1), 53–60.

Jackson, 2010. Genotyping Protocols Database, Protocol for Genotyping TC1 Mice Available at: http://jaxmice.jax.org/protocolsdb/f?p=116:2:1100215068681904::NO:2:P2_MASTER_PROTOCOL_ID, P2_JRS_CODE:4801,010801.

Kleschevnikov, A.M., et al., 2012. Deficits in cognition and synaptic plasticity in a mouse model of Down syndrome ameliorated by GABAB receptor antagonists. J. Neurosci. 32 (27), 9217–9227 (Available at: http://www.ncbi.nlm.nih.gov/pubmed/22764230).

Lamas, J.A., Selyanko, A.A., Brown, D.A., 1997. Effects of a cognition-enhancer, linopirdine (DuP 996), on M-type potassium currents (I(K(M))) and some other voltage- and ligand-gated membrane currents in rat sympathetic neurons. Eur. J. Neurosci. 9, 605–616.

Li, B., et al., 2012. Role of HCN channels in neuronal hyperexcitability after subarachnoid hemorrhage in rats. J. Neurosci. 32 (9), 3164–3175 (Available at: http://www.ncbi.nlm.nih.gov/pubmed/22378889).

Lorenzi, H.A., Reeves, R.H., 2006. Hippocampal hypocellularity in the Ts65Dn mouse originates early in development. Brain Res. 1104 (1), 153–159.

Lorenzi, H., et al., 2010. PCR prescreen for genotyping the Ts65Dn mouse model of Down syndrome. Biotechniques 48 (1), 35–38 (Available at: http://www.ncbi.nlm.nih.gov/pubmed/20095097).

Lorenzon, N.M., Foehring, R.C., 1992. Relationship between repetitive firing and afterhyperpolarizations in human neocortical neurons. J. Neurophysiol. 67 (2), 350–363 (Available at: http://www.ncbi.nlm.nih.gov/pubmed/1373765).

Martinez-Cue, C., et al., 2002. Differential effects of environmental enrichment on behavior and learning of male and female Ts65Dn mice, a model for Down syndrome. Behav. Brain Res. 134 (1–2), 185–200 (Available at: http://www.ncbi.nlm.nih.gov/pubmed/12191805).

Migliore, M., 2012. CA1 Pyramidal Neuron: Ih Current Available at: http://senselab.med.yale.edu/ModelDB/ShowModel.asp?model=144541&file=\Ih_current\readme.html.

Migliore, M., Migliore, R., 2012. Know your current I(h): interaction with a shunting current explains the puzzling effects of its pharmacological or pathological modulations. PLoS One 7 (5), e36867 (Available at: http://www.ncbi.nlm.nih.gov/pubmed/22606301).

Mitra, A., Blank, M., Madison, D.V., 2012. Developmentally altered inhibition in Ts65Dn, a mouse model of Down syndrome. Brain Res. 1440, 1–8.

Morice, E., et al., 2008. Preservation of long-term memory and synaptic plasticity despite short-term impairments in the Tc1 mouse model of Down syndrome. Learn. Mem. 15 (7), 492–500 (Available at: http://www.ncbi.nlm.nih.gov/pubmed/18626093).

O'Doherty, A., et al., 2005. An aneuploid mouse strain carrying human chromosome 21 with Down syndrome phenotypes. Science 309 (5743), 2033–2037 (Available at: http://www.ncbi.nlm.nih.gov/pubmed/16179473).

Orozco, C.B., et al., 1987. Electrophysiological properties of cultured dorsal root ganglion and spinal cord neurons of normal and trisomy 16 fetal mice. Brain Res. 429 (1), 111–122 (Available at: http://www.ncbi.nlm.nih.gov/pubmed/2952222).

Orozco, C.B., Epstein, C.J., Rapoport, S.I., 1988. Voltage-activated sodium conductances in cultured normal and trisomy 16 dorsal root ganglion neurons from the fetal mouse. Brain Res. 466 (2), 265–274 (Available at: http://www.ncbi.nlm.nih.gov/pubmed/2452000).

Papa, M., et al., 1995. Morphological analysis of dendritic spine development in primary cultures of hippocampal neurons. J. Neurosci. 15 (1 Pt 1), 1–11 (Available at: http://www.ncbi.nlm.nih.gov/pubmed/7823120).

Peretz, A., et al., 2005. Meclofenamic acid and diclofenac, novel templates of KCNQ2/Q3 potassium channel openers, depress cortical neuron activity and exhibit anticonvulsant properties. Mol. Pharmacol. 67 (4), 1053–1066 (Available at: http://www.ncbi.nlm.nih.gov/pubmed/15598972).

Pinter, J.D., et al., 2001. Amygdala and hippocampal volumes in children with Down syndrome: a high-resolution MRI study. Neurology 56, 972–974.

Reeves, R.H., 2006. Down syndrome mouse models are looking up. Trends Mol. Med. 12 (6), 237–240 (Available at: http://www.ncbi.nlm.nih.gov/pubmed/16677859).

Reeves, R.H., et al., 1995. A mouse model for Down syndrome exhibits learning and behaviour deficits. Nat. Genet. 11 (2), 177–184 (Available at: http://www.ncbi.nlm.nih.gov/pubmed/7550346).

Reimann, F., Ashcroft, F.M., 1999. Inwardly rectifying potassium channels. Curr. Opin. Cell Biol. 11 (4), 503–508.

Reinholdt, L.G., et al., 2011. Molecular characterization of the translocation breakpoints in the Down syndrome mouse model Ts65Dn. Mamm. Genome 22 (11–12), 685–691 (Available at: http://www.ncbi.nlm.nih.gov/pubmed/21953412).

Roizen, N.J., Patterson, D., 2003. Down's syndrome. Lancet 361 (9365), 1281–1289 (Available at: http://www.ncbi.nlm.nih.gov/pubmed/12699967).

Rueda, N., Florez, J., Martinez-Cue, C., 2012. Mouse models of Down syndrome as a tool to unravel the causes of mental disabilities. Neural Plast. 2012, 584071 (Available at: http://www.ncbi.nlm.nih.gov/pubmed/22685678).

Sago, H., et al., 2000. Genetic dissection of region associated with behavioral abnormalities in mouse models for Down syndrome. Pediatr. Res. 48 (5), 606–613.

Salehi, A., et al., 2007. Using mouse models to explore genotype–phenotype relationship in Down syndrome. Ment. Retard. Dev. Disabil. Res. Rev. 13 (3), 207–214 (Available at: http://www.ncbi.nlm.nih.gov/pubmed/17910089).

Scott, B.S., et al., 1981. Abnormal electric membrane properties of Down's syndrome DRG neurons in cell culture. Brain Res. 254 (2), 257–270 (Available at: http://www.ncbi.nlm.nih.gov/pubmed/6456037).

Shibata, R., et al., 2000. A-type K+ current mediated by the Kv4 channel regulates the generation of action potential in developing cerebellar granule cells. J. Neurosci. 20 (11), 4145–4155 (Available at: http://www.ncbi.nlm.nih.gov/pubmed/10818150).

Singh, N.A., et al., 1998. A novel potassium channel gene, KCNQ2, is mutated in an inherited epilepsy of newborns. Nat. Genet. 18 (1), 25–29 (Available at: http://www.ncbi.nlm.nih.gov/pubmed/9425895).

Vieregge, P., et al., 1992. Late cognitive event-related potentials in adult Down's syndrome. Biol. Psychiatry 32 (12), 1118–1134 (Available at: http://www.ncbi.nlm.nih.gov/pubmed/1477192).

Wenger, G.R., Schmidt, C., Davisson, M.T., 2004. Operant conditioning in the Ts65Dn mouse: learning. Behav. Genet. 34 (1), 105–119 (Available at: http://www.ncbi.nlm.nih.gov/pubmed/14739701).

Wulff, H., Zhorov, B.S., 2008. K+ channel modulators for the treatment of neurological disorders and autoimmune diseases. Chem. Rev. 108 (5), 1744–1773 (Available at: http://www.ncbi.nlm.nih.gov/pubmed/18476673).

Yuan, W., Burkhalter, A., Nerbonne, J.M., 2005. Functional role of the fast transient outward K+ current IA in pyramidal neurons in (rat) primary visual cortex. J. Neurosci. 25, 9185–9194.